Batteries & Supercaps

Research Article
doi.org/10.1002/batt.202100319

Chemistry Europe
European Chemical Societies Publishing

www.batteries-supercaps.org

Crosslinked Polymer-Brush Electrolytes: An Approach to Safe All-Solid-State Lithium Metal Batteries at Room Temperature

Xiaoyu Ji,[a, b] Shimei Li,[c] Mengxue Cao,[d] Ruiqi Liang,[d] Lin-Lin Xiao,[b] Kan Yue,[b, e] Shaohong Liu,[c] Xingui Zhou,[a] and Zi-Hao Guo*[b, e]

Electric vehicles, intelligent machines, and portable electronics in our daily lives are placing insatiable demand on safe and powerful battery materials that can function at room temperature. Herein, we report an ultrathin and robust solid-state electrolyte with crosslinked polymer-brush architecture. On one hand, the highly mobile polymer brushes with a moderate side chain length enable efficient cation solvation and fast ion transport, offering room-temperature ionic conductivity as high as 0.23 mS cm^{-1}. On the other hand, incorporation of the inorganic core crosslinker endows the material with enhanced mechanical strength, thermal stability, and fire resistance. As a result, the crosslinked polymer-brush electrolyte films demonstrate stable lithium electrodeposition and great electrochemical performance in Li/$LiFePO_4$ cells at 30 °C, providing a promising pathway to next-generation safe and high-energy lithium metal batteries.

1. Introduction

Unprecedented progress in low-carbon transition, portable electronics, and autonomous machines places growing demand for safe, cost-effective yet energy-dense electrical energy storage devices.[1–4] Compared to today's lithium-ion batteries (LIBs), lithium metal batteries (LMBs) offer the higher anode capacity, lower electrochemical potential, and allow the use of sulfur or air cathodes to achieve higher energy density, having become a highly sought-after pathway to such devices.[5,6] However, commercialization of LMBs lags far behind LIBs due to the chemical and morphological instabilities of metallic lithium (Li) anodes, which result in uneven Li electrodeposition and uncontrollable dendrite growth.[7,8] These dendrites propagate during charge-discharge cycles and short-circuit the cells, especially in cells based on organic liquid electrolytes (LEs),[9] leading to safety concerns such as leakage, fire, and explosion. Taking advantages of enhanced chemical and mechanical stabilities, solid-state electrolytes (SSEs) have emerged as an ideal solution to tackle these challenges and fabricated LMBs with high safety, energy density and long-term stability.[10,11]

While inorganic ceramic electrolytes provide high ionic conductivity, they show poor mechanical compliance and interfacial compatibility with electrodes.[12] Alternatively, polymer materials are being intensely pursued as they exhibit low cost, easy processability, and can compensate the electrode volume changes through their elastic and plastic deformation.[13–15] However, ion transport in polymer conductors relies on their segmental relaxation, which is slower than the required rate for practical battery application.[16] Thus, scalable polymer engineering strategies have developed to improve their ionic conductivity. One eminent strategy is based on block copolymer architectures, i.e., poly(ethylene oxide)-*b*-polystyrene (PEO-*b*-PS),[17–19] in which the ion-conductive PEO block melts at elevated temperature to fast transport ions and the stiff PS block provides requisite mechanical support. Unfortunately, this method mainly aims to overcome the trade-off between ionic conductivity and mechanical properties at high temperatures, limiting their application in numerous state-of-the-art electrical devices that need to function at room temperature. Other prevailing strategies include physically or chemically crosslinking,[20–25] graft polymers,[26–30] inorganic fillers doping,[31–33] and otherwise. Many of these materials have presented graceful performance in LMBs, but their eligible conductivity ($\geq$0.1 mS cm^{-1}) tends to rely on LE additives, translating to potential safety risk for use in human life. Designing more judicious architectures to further facilitate the polymer segmental dynamics and promote their room-temper-

[a] X. Ji, Prof. X. Zhou
Science and Technology on Advanced Ceramic Fibers and Composites Laboratory, College of Aerospace Science and Engineering
National University of Defense Technology
Changsha 410073, China
[b] X. Ji, L.-L. Xiao, Prof. K. Yue, Prof. Z.-H. Guo
South China Advanced Institute for Soft Matter Science and Technology, School of Molecular Science and Engineering
South China University of Technology
Guangzhou 510640, China
E-mail: guozihao@scut.edu.cn
[c] S. Li, Prof. S. Liu
PCFM Lab, School of Chemistry
Sun Yat-sen University
Guangzhou 510275, China
[d] M. Cao, R. Liang
Department of Chemical and Environmental Engineering
Yale University
New Haven, Connecticut 06511, USA
[e] Prof. K. Yue, Prof. Z.-H. Guo
Guangdong Provincial Key Laboratory of Functional and Intelligent Hybrid Materials and Devices
South China University of Technology
Guangzhou, 510640, China

Supporting information for this article is available on the WWW under https://doi.org/10.1002/batt.202100319

Research Article
doi.org/10.1002/batt.202100319
Chemistry Europe
European Chemical Societies Publishing

ature ionic conductivity is the key point to get rid of high temperatures or additional LEs.

Recently, we designed an efficient room-temperature Li ion (Li^+) conductor with mixed-graft block copolymer (mGBCP) structure, in which the high mobility of the short PEO brushes and free PEO chains signicantly accelerates the Li^+ migration rate.[28,34] However, owing to intrinsic softness of brush polymers,[35,36] such SSE exhibits low storage modulus of ca. 0.1 MPa, limiting their long-time cycling stability in LMBs. The recently developed crosslinked polymeric networks (Scheme 1a) that demonstrate enhanced mechanical property and dendrite suppression seem to provide a promising method to overcome this issue.[21,24,25,37]

Herein, we report a crosslinked polymer-brush electrolyte (CPBE) that inherits the merits of crosslinked network and polymer-brush architecture (Scheme 1b). Polyhedral oligomeric silsesquioxane (POSS), a hard and easily available inorganic material, is selected as not only a crosslinker but also mechanical reinforcing cores to compensate the softness of the polymer-brush architecture. Simultaneously, the PEO brushes maintain the high mobility and provide superior ionic conductivity. Moreover, a non-monotonic correlation between ionic conductivity and side chain length of brush polymer electrolytes is revealed, which is ascribed to a competitive effect between the segmental dynamics of entire side chains and the gradient distribution of cation solvation probability and segmental mobility along the side chains. With enhanced ionic conductivity, mechanical and thermal stabilities, ultrathin CPBE membranes are in situ prepared on Li anodes and cathode materials, endowing the assembled all-solid-state LMBs with great safety, energy density, and electrochemical performance at room temperature.

2. Results and Discussion

Figure 1(a) depicts a schematic of the synthetic procedure to create the CPBE membranes. It is a versatile one-pot photopolymerization using poly(ethylene oxide) acrylate (macromonomer), octa-functional POSS acrylate (crosslinker) and irgacure 2959 (photo initiator), in the presence of poly(ethylene oxide) monomethyl ether free PEO chains (solid state at room temperature), bis(trifluoromethane) sulfonamide lithium (LiTFSI) salt and tetrahydrofuran (THF) solvent. Since all materials show good chemical stability with electrode materials, the mixtures can be casted onto not only inert Teflon (PTFE) substrates to manufacture free-standing films, but also active electrode materials to capture better interfacial contacts. After casting the solution on substrates, we firstly heated it to 55 °C to slowly evaporate the THF that has unneglectable effect on the electrochemical properties but is difficult to thoroughly remove from the as-crosslinked networks.[38] At identical temperature, a low-viscosity flowing state of the solvent-free system enabled the high reactivity of reactants, and the final photopolymerization was triggered by exposing the acrylate groups to ultraviolent (UV) light ($\lambda = 352$ nm).

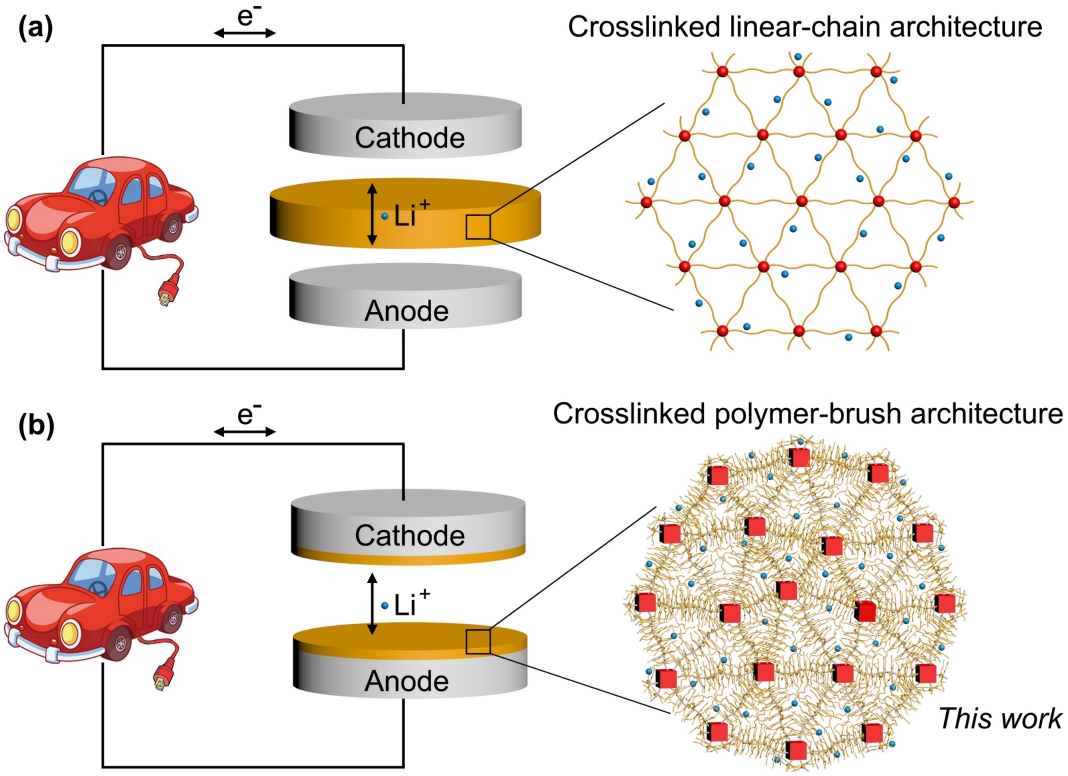

Scheme 1. Schematic illustrations of the batteries with a) crosslinked linear-chain polymer electrolyte and b) our ultrathin solid-state electrolyte with crosslinked polymer-brush architecture.

Research Article
doi.org/10.1002/batt.202100319
Chemistry Europe
European Chemical Societies Publishing

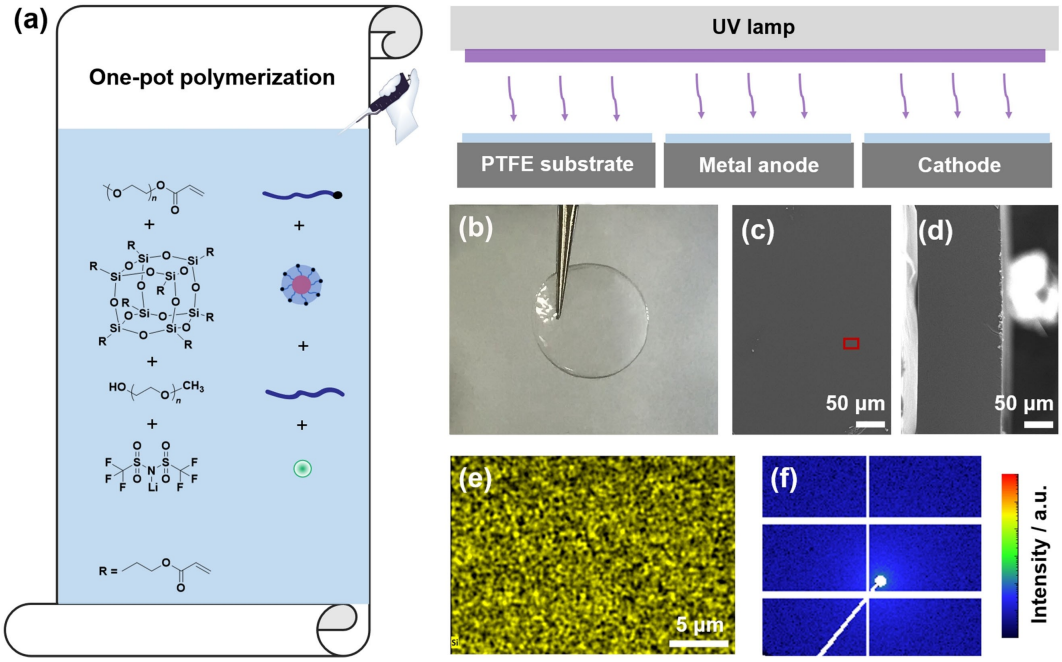

Figure 1. a) Schematic diagram of the synthetic procedure to CPBE films on various substrates; b) optical image of the free-standing CPBE750 film; c, d) SEM images of the surface and cross-section of the CPBE750 film; e) EDS elemental mapping of Si taken from the red rectangle in panel (c); f) 2D SAXS profile of the CPBE750.

Remarkably, this route can readily produce membranes with controllable thickness by regulating the solution concentration, providing a facile approach to ultrathin SSE films. Here, free-standing CPBE films with thickness of ca. 140 and 20 μm are displayed in Figures 1b and S1, respectively, which are transparent, homogenous, and without observable aggregation. Moreover, mechanical strength of the CPBEs is also highly adjustable via the balance between the tough POSS crosslinked polymer-brush structure and the soft free PEO component (Table S1). For simplicity, fixed mass fractions of PEO brush, POSS crosslinker, and free PEO chain of 45%, 15%, and 40% are maintained, accompanying with a molar ratio of Li^+ to ethylene oxide (EO) of 0.05. The number average molecular weight (M_n) of the free PEO chain is 750 Da. The CPBEs with various brush side chain length are denoted as CPBE*n*, in which *n* is the M_n of the macromonomer.

Evolution of the chemical bonding and composition was investigated by Fourier transform infrared spectroscopy (FTIR) and nuclear magnetic resonance (NMR). The FTIR results (Figures S2 and S3) show that the C=C bonds at ca. 1650 cm^{-1} presenting in macromonomers and crosslinkers disappears in CPBEs, indicating the acrylate groups have efficiently reacted. Furthermore, the CPBEs were immersed in deuterochloroform ($CDCl_3$) (over 1 hour) to extract the soluble components and the $CDCl_3$ solution was examined by ^1H NMR. No signals of acrylates but only free PEO chains are detected (Figure S7), illustrating the PEO macromonomers and POSS crosslinkers are completely converted into the crosslinked network that hosts the free PEO chains. Notably, due to the pre-evaporation step, the THF solvent can be removed before polymerization (Figures S8 and S9), and thus no THF residual is detected in the CPBEs. The structural homogeneity of CPBE films was studied by scanning electron microscope (SEM) and small-angle X-ray scattering (SAXS). As shown in Figure 1(c and d), SEM images of surface and cross-section show smooth and compact textures of the CPBE films. Energy dispersive spectroscopy (EDS) of the silicon elemental mapping (Figure 1e) demonstrates the uniform distribution of the inorganic POSS core crosslinkers. The homogeneous nature of CPBE films is further evidenced by 2D SAXS pattern (Figure 1f), in which no aggregation and phase separation scatterings is observed.

Ionic conductivity of the CPBEs with various side chain length was studied at 25 °C and plotted in Figure 2(a) and Table S4. Interestingly, the ionic conductivity of CPBEs demonstrates a non-monotonic variation, which increases from CPBE350 to CPBE 750 and decreases from CPBE750 to CPBE2000. In order to further confirm and explore this phenomenon in polymer-brush electrolytes, pure polymer-brush (PPB*n*) and crosslinked polymer-brush (CPB*n*) architectures without the free PEO chains were synthesized and blended with Li salt (*n* denotes the various side chain length). As shown in Figure 2(a), ionic conductivity of the PPBs and CPBs changes with the side chain length similar as the CPBEs do, indicating a significant impact of the side chain length on ionic conductivity. To gain a better insight into the ion transport mechanism of the polymer-brush architectures, differential scanning calorimeter (DSC) was employed to study their thermodynamic properties. CPB350, CPB750 and CPB2000 were tested and the corresponding DSC curves are depicted in Figure 2(b). Since the influence of free PEO chains is excluded in CPBs, these samples exhibit T_g and melting points (T_m) that

Research Article
doi.org/10.1002/batt.202100319
Chemistry Europe
European Chemical Societies Publishing

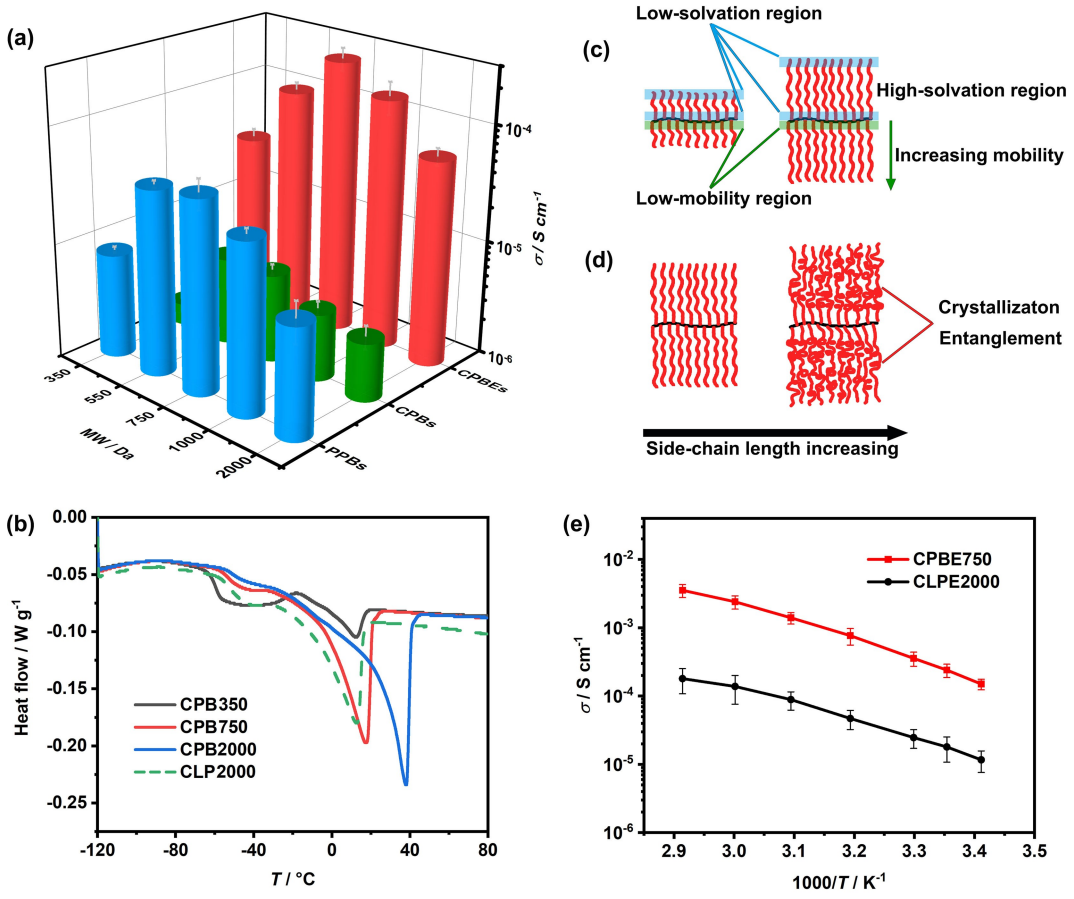

Figure 2. a) Ionic conductivity of CPBEs, CPBs, and PPBs with the various side chain length at 25 °C; b) DSC profiles of CLP2000 and CPBs with various side chain lengths; c, d) schematics illustrating the heterogeneous distribution of Li^+ solvation probability and segmental mobility along the PEO side chains (c), and the various side chain topology with the increase of side chain length (d); e) ionic conductivity of CLPE2000 and CPBE750 as a function of temperature.

are dictated by their side chains, exhibiting a monotonic increase with the side chain length (Table S5).

It is known that ion transport in polyether-based electrolytes is intrinsically coupled to their segmental dynamics and governed by the Vogel-Tamman-Fulcher (VTF) relationship. The VTF equation instructs that a lower T_g of the polymer matrix determines a facilitated segmental dynamics and enhanced ionic conductivity.[39] However, while the T_g decreases from CPB750 (−51 °C) to CPB350 (−61 °C), their ionic conductivity exhibits a descending tendency. This T_g-decoupled ionic conductivity at a low side chain length range (below 750 Da) originates from the heterogeneous Li^+ solvation probability and segmental mobility along the side chains. Ionic conductivity (σ) of a polymer electrolyte is a product of the concentration of free charge carriers (c) and the mobility (μ) at which the ions can move via segmental relaxation and ion hopping: $\sigma = \mu c$. One the one hand, segmental dynamics (μ) of the polymer-brush architectures exhibit a gradient distribution along the side chain. As shown in Figure 2(c), one end of the side chain in PEO brush is chemically fixed to the backbone whereas another one (tail) is free, leading to an increasing segmental mobility from the EOs close to backbone to those near the tails. Specifically, recent calculations suggest that the relaxation time of different EOs in PEO graft polymers spans even three orders of magnitude from the backbone to side chain tails.[40,41] Such heterogeneous segmental dynamics cause that, within a certain scale, the longer side chains contain more proportion of highly mobile EOs, and therefore perform higher conductivity. One the other hand, the c in PEO-based electrolytes depends on the cation solvation by polymer chains, which commonly requires either one single chain with six contiguous EOs or two chains each with three contiguous EOs to coordinate with Li^+.[42,43] With regard to brush polymers, simulation studies found that the middle of the side chains offer more permutations to form the contiguous six or three EO solvating segments to complex Li^+, whereas the positions near the backbone and side chain tails share the less solvation probability.[44,45] As a result, the polymer brush with shorter side chain length, especially with 350 Da or less that holds only a few EO units, has lower fraction of effective solvation sites, leading to a decrease of c. Synergistically, the enhancement of μ and c results in the increased ionic conductivity with the side chain length.

With the side chain length further increases (Figure 2d), the effect of heterogeneity of Li^+ solvation and segmental relaxation along the side chains is diluted and diminished. The ionic conductivity becomes dominated by the segmental dynamics of the whole side chains, which is strongly coupled to their T_g, entanglement, and crystallization. While the T_g

Research Article
doi.org/10.1002/batt.202100319
Chemistry Europe
European Chemical Societies Publishing

exhibits only a minor increase from CPB750 (−51 °C) to CPB2000 (−45 °C), the T_m increases significantly from CPB750 (12 °C) to CPB2000 (38 °C). It implies that at room temperature the PEO side chains present a highly mobile melt state in CPB750, but begin to crystallize with the side chain length enlarging to 2000 Da. Wide angle X-ray diffraction (WAXD) (Figures S11 and S12) further proves such crystallization behavior. While the CPBEs with side chain length below 1000 Da are amorphous at room temperature, CPBE2000 shows obvious PEO crystallization. In addition, PEO chains exhibit an entanglement molecular weight (M_e) of 1700–2000 Da,[46] indicating that the PEO-brush architecture could become more entangled with the side chain length increasing to kDa scope. Therefore, the decrease of ionic conductivity from CPB750 to CPB2000 is attributed to the side chain entanglement and crystallization, which hinders the ion transport.

Overall, a competitive impact between the heterogeneity of c and μ along the side chains and the segmental dynamics of the whole side chains on ionic conductivity is revealed in polymer-brush architectures. Beyond that, recent reports suggest decrease of the PEO chain length from 2000 to 750 Da in crosslinked linear-chain architectures leads to a reduction of ionic conductivity,[22,47] indicating the ion-conducting heterogeneity along polymer chains could also exist in crosslinked linear-chain networks, where the EOs near the crosslinking junctions exhibit lowered segmental mobility and solvation probability.

Compared to the crosslinked linear-chain networks, the advantage of crosslinked polymer-brush architectures is the enhanced flexibility of the single-end-tethered PEO side chains rather than the double-end-fixed linear PEO chains. For comparison, a double-end-fixed crosslinked linear PEO electrolyte (CLPE2000) with the same POSS/PEO/LiTFSI contents as CPBEs was synthesized. DSC (Figure 2b) and WAXD (Figure S10) results illustrate that the crystallization of PEO chains disappears in CLPE2000. Both in amorphous state, as expected, the more flexible single-end-tethered CPBE750 demonstrates ionic conductivity (0.23 mS cm^{-1} at room temperature) over one order of magnitude higher than that of the double-end-fixed CLPE2000 (Figure 2e).

One key factor of polymer-based SSEs is their mechanical performance and dendrite resistibility. With optimal ionic conductivity, CPBE750 films were in situ polymerized on lithium anodes and $LiFePO_4$ cathodes, with a thickness of ca. 20 μm and a flat surface on nanoscale (Figure 3a–c). The stiff POSS acting as both crosslinker and mechanical reinforcement endows the films with high Young's modulus of ca. 57 MPa by atomic force microscopy (AFM) mapping (Figure 3d). Symmetric Li|CPBE750|Li cells were then assembled to evaluate their dendrite resistibility. As shown in Figure 3(e), stable stripping/plating cycling for over 500 cycles is achieved under 0.1 mA cm^{-2} at 30 °C, indicating an even Li electrodeposition and suppressed dendrite growth. In contrast, the commercial liquid electrolyte operation (50 μm in thickness) leads to the short circuit within less than 100 cycles (Figure S17). Moreover,

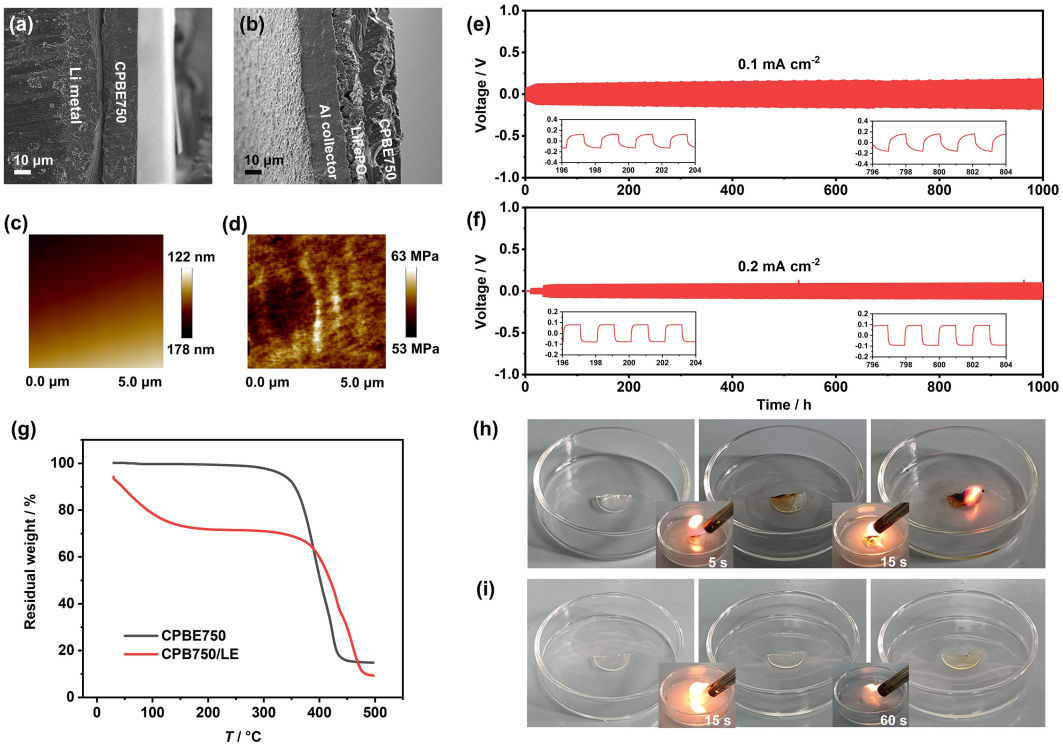

Figure 3. SEM images of the CPBE750 film in situ prepared on a) Li metal anode and b) $LiFePO_4$ cathodes; c) AFM height mapping and d) Young's modulus mapping of the in-situ prepared CPBE750 film; voltage profiles of symmetric Li|CPBE750|Li cells at e) 0.1 mA cm^{-2}, 30 °C and f) 0.2 mA cm^{-2}, 60 °C; g) TGA curves of the CPBE750 with free PEO chain and commercial LE; combustion tests of the CPBE750 with h) free PEO chains and i) commercial LEs.

after raising operation temperature to 60 °C, the CPBE750 exhibits great cycling stability as well (over 500 cycles at 0.2 mA cm^{-2}, Figure 3f), demonstrating that the mechanical stiffness of the crosslinked polymer-brush architectures does not degrade at elevated temperatures as the traditional linear PEO electrolytes (short circuit within 20 cycles at 60 °C).[48] The robust molecular network crosslinked by hard POSS cores plays the pivotal role in the stable Li electrodeposition and the prevention of dendrite growth.

Thermostability is another key factor of SSEs for battery safety. Since most of battery fires or explosions were caused by the usage of organic LEs, thermogravimetric analysis (TGA) and combustion tests were conducted to compare the heat endurance of CPBE750 and the widely studied crosslinked network/LE systems. As shown in Figure 3(g), our CPBE750 that hosts 40% PEO free chain exhibits excellent thermal stability with no mass loss up to 300 °C, significantly reducing the risk of security incidents. On the contrary, the crosslinked polymer-brush network that contains 40% LE (CPB750/LE) undergoes dramatic mass loss from room temperature, owing to the fast evaporation of the volatile LEs. Similar results could also be found in CLP2000/LE (Figure S14) and other crosslinked network/LE systems.[49] Combustion tests recognised the superior fire resistance of the CPBE750. While the CPB750/LE burns after being exposed to butane flame within 15 s (Figure 3h), the CPBE750 cannot be ignited over 1 min (Figure 3i). The enhancement of thermal stability and flame retardance arises from the replacement of flammable LEs with the stable solid-state free PEO chains (Figures S15 and S16). Meanwhile, the incorporation of POSS inorganic cores also plays a key role in the reduced combustibility in nanohybrid polymer materials.[50,51]

Electrochemical performance of the in situ prepared CPBE750 was examined in Li|LiFePO$_4$ full cells. The batteries were cycled at 30 °C with charge/discharge rates from *C*/10 to *C*/1, where the *C*/*x* represents a charge or discharge cycle of theoretical cathode capacity (*C*, 170 mAh g^{-1} for LiFePO$_4$) in *x* hours. As shown in Figure 4(a), well-defined potential plateaus are observed at charge/discharge rates up to C/2, with high capacities of 161 mAh g^{-1} at *C*/10 and 147 mAh g^{-1} at *C*/2, respectively. Increase of the rate to *C*/1 results in a deteriorated rate performance, which could be attributed to the unstable Li electrodeposition at elevated current density (Figure S18). Nevertheless, when the rate is switched back to *C*/10, the capacity retention is as high as 92% of the starting value (Figure 4b). For comparison, properties of recent research on PEO-based electrolytes were summarized in Table S6. Several state-of-the-art ones have achieved high capacity of ca. 160 mAh g^{-1} and great long-lasting stability, albeit high operating temperature or LE additives have generally to be employed. Moreover, most of current SSEs used in LMBs are with thickness of 100–300 μm, which is too thick for the pursuit of batteries with high volume energy density.[52] The ultrathin CPBEs demonstrated here provide an exciting avenue for room-temperature all-solid-state LMBs with enhanced safety and energy density.

3. Conclusions

In summary, a class of fast lithium-ion conductors, CPBEs, are synthesized through crosslinked polymer-brush architectures. Compared to crosslinked linear-chain networks, the single-end-tethered side chains in CPBEs offer more free volumes, achieving higher segmental mobility and ionic conductivity. Ionic conductivity of such polymer-brush electrolytes is proved to depend on their side chain length. Within a short-length range, the heterogeneous distribution of the segmental mobility and cation solvation probability along the side chains leads to the ionic conductivity increasing with the side chain length, whereas at a long-length scope the increasing entanglement and crystallization with the side chain length results in a decrease of the ionic conductivity. Incorporation of inorganic POSS cores grants the CPBEs enhanced mechanical strength (57 MPa), thermal stability (≥300 °C in air), and fire resistance (≥60 s under butane flame). With improved ionic conductivity and mechanical and thermal stabilities, the resulting ultrathin CPBE films (20 μm) demonstrate stable Li electrodeposition over 500 cycles and superior electrochemical performance in all-solid-state LMBs, affording a fascinating material design for room-temperature electrical energy storage and modern battery industry.

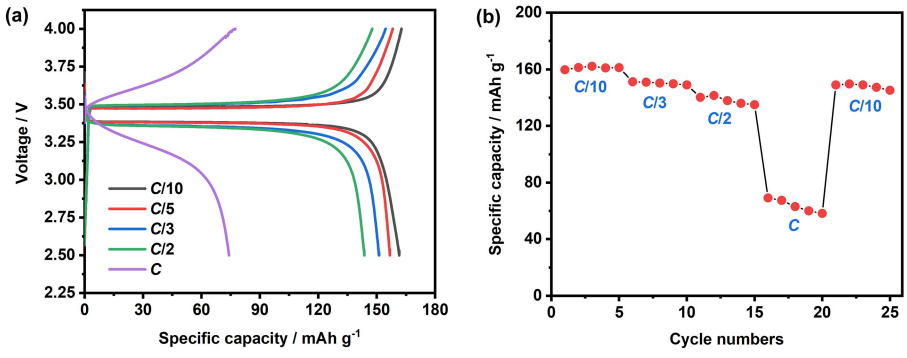

Figure 4. a) Rate and b) cycling performance of all-solid-state Li|LiFePO$_4$ batteries with the ultrathin CPBE films at 30 °C.

Experimental Section

The Experimental Section is available in the Supporting Information.

Acknowledgements

This work is supported by the National Natural Science Foundation of China (No. 22003017), Natural Science Foundation of Guangdong Province (2020A1515011506) and the Recruitment Program of Guangdong (2016ZT06C322). X.J. is thankful for the financial support from the China Scholarship Council (No. 201903170199) for his visit to Yale University. The authors thank Prof. Dingcai Wu (Sun Yat-sen University), Prof. Mingjiang Zhong (Yale University), and Prof. Stephen Z. D. Cheng (University of Akron) for helpful discussion. The authors also thank Prof. Shangda Jiang, Prof. Mingjun Huang and Dr. Shen Zhou (South China University of Technology) for their assistance in facility supports. Valuable time provided by Designer Alissa Y. Liu for cartoon guidance is appreciated as well.

Conflict of Interest

The authors declare no conflict of interest.

Keywords: energy density · lithium batteries · ionic conductivity · room temperature · solid-state electrolyte

[1] J. Markard, *Nat. Energy* **2018**, *3*, 628–633.
[2] Z. P. Cano, D. Banham, S. Ye, A. Hintennach, J. Lu, M. Fowler, Z. Chen, *Nat. Energy* **2018**, *3*, 279–289.
[3] B. Chu, W. Burnett, J. W. Chung, Z. Bao, *Nature* **2017**, *549*, 328–330.
[4] M. Wang, D. Vecchio, C. Wang, A. Emre, X. Xiao, Z. Jiang, P. Bogdan, Y. Huang, N. A. Kotov, *Sci. Rob.* **2020**, *5*, eaba1912.
[5] J. W. Choi, D. Aurbach, *Nat. Rev. Mater.* **2016**, *1*, 16013.
[6] P. G. Bruce, S. A. Freunberger, L. J. Hardwick, J.-M. Tarascon, *Nat. Mater.* **2012**, *11*, 19–29.
[7] X. Sun, X. Zhang, Q. Ma, X. Guan, W. Wang, J. Luo, *Angew. Chem. Int. Ed.* **2020**, *59*, 6665–6674; *Angew. Chem.* **2020**, *132*, 6730–6739.
[8] D. Cao, X. Sun, Q. Li, A. Natan, P. Xiang, H. Zhu, *Matter* **2020**, *3*, 57–94.
[9] M. Nojabaee, D. Kopljar, N. Wagner, K. A. Friedrich, *Batteries & Supercaps* **2021**, *4*, 909–922; Supercaps **2021**, 4, 909–922.
[10] Q. Zhao, S. Stalin, C.-Z. Zhao, L. A. Archer, *Nat. Rev. Mater.* **2020**, *5*, 229–252.
[11] Z. Hu, G. Li, A. Wang, J. Luo, X. Liu, *Batteries & Supercaps* **2019**, *3*, 331–335.
[12] Z. Gao, H. Sun, L. Fu, F. Ye, Y. Zhang, W. Luo, Y. Huang, *Adv. Mater.* **2018**, *30*, 1705702.
[13] D. T. H. Jr., N. P. Balsara, *Annu. Rev. Mater. Res.* **2013**, *43*, 503–525.
[14] D. Zhou, D. Shanmukaraj, A. Tkacheva, M. Armand, G. Wang, *Chem* **2019**, *5*, 2326–2352.
[15] J. Lopez, D. G. Mackanic, Y. Cui, Z. Bao, *Nat. Rev. Mater.* **2019**, *4*, 312–330.
[16] V. Bocharova, A. P. Sokolov, *Macromolecules* **2020**, *53*, 4141–4157.
[17] G. M. Stone, S. A. Mullin, A. A. Teran, D. T. Hallinan, A. M. Minor, A. Hexemer, N. P. Balsara, *J. Electrochem. Soc.* **2012**, *159*, A222–A227.
[18] R. Bouchet, S. Maria, R. Meziane, A. Aboulaich, L. Lienafa, J.-P. Bonnet, T. N. T. Phan, D. Bertin, D. Gigmes, D. Devaux, R. Denoyel, M. Armand, *Nat. Mater.* **2013**, *12*, 452–457.
[19] D. Sharon, P. Bennington, M. A. Webb, C. Deng, J. J. de Pablo, S. N. Patel, P. F. Nealey, *J. Am. Chem. Soc.* **2021**, *143*, 3180–3190.
[20] R. Khurana, J. L. Schaefer, L. A. Archer, G. W. Coates, *J. Am. Chem. Soc.* **2014**, *136*, 7395–7402.
[21] S. Choudhury, R. Mangal, A. Agrawal, L. A. Archer, *Nat. Commun.* **2015**, *6*, 10101.
[22] Q. Pan, D. M. Smith, H. Qi, S. Wang, C. Y. Li, *Adv. Mater.* **2015**, *27*, 5995–6001.
[23] D. G. Mackanic, X. Yan, Q. Zhang, N. Matsuhisa, Z. Yu, Y. Jiang, T. Manika, J. Lopez, H. Yan, K. Liu, X. Chen, Y. Cui, Z. Bao, *Nat. Commun.* **2019**, *10*, 5384.
[24] S. Choudhury, S. Stalin, D. Vu, A. Warren, Y. Deng, P. Biswal, L. A. Archer, *Nat. Commun.* **2019**, *10*, 4398.
[25] X. Li, Y. Zheng, C. Y. Li, *Energy Storage Mater.* **2020**, *29*, 273–280.
[26] P. E. Trapa, Y.-Y. Won, S. C. Mui, E. A. Olivetti, B. Huang, D. R. Sadoway, A. M. Mayes, S. Dallek, *J. Electrochem. Soc.* **2005**, *152*, A1.
[27] J. Sun, G. M. Stone, N. P. Balsara, R. N. Zuckermann, *Macromolecules* **2012**, *45*, 5151–5156.
[28] X. Ji, M. Cao, X. Fu, R. Liang, A. N. Le, Q. Zhang, M. Zhong, *Giant* **2020**, *3*, 100027.
[29] M. Jia, P. Wen, Z. Wang, Y. Zhao, Y. Liu, J. Lin, M. Chen, X. Lin, *Adv. Funct. Mater.* **2021**, *31*, 2101736.
[30] M. Zhou, R. Liu, D. Jia, Y. Cui, Q. Liu, S. Liu, D. Wu, *Adv. Mater.* **2021**, *33*, 2100943.
[31] F. Croce, G. B. Appetecchi, L. Persi, B. Scrosati, *Nature* **1998**, *394*, 456–458.
[32] S. Qian, H. Chen, Z. Wu, D. Li, X. Liu, Y. Tang, S. Zhang, *Batteries & Supercaps* **2020**, *4*, 39–59.
[33] S. Li, S.-Q. Zhang, L. Shen, Q. Liu, J.-B. Ma, W. Lv, Y.-B. He, Q.-H. Yang, *Adv. Sci.* **2020**, *7*, 1903088.
[34] Z.-H. Guo, A. N. Le, X. Feng, Y. Choo, B. Liu, D. Wang, Z. Wan, Y. Gu, J. Zhao, V. Li, C. O. Osuji, J. A. Johnson, M. Zhong, *Angew. Chem. Int. Ed.* **2018**, *57*, 8493–8497; *Angew. Chem.* **2018**, *130*, 8629–8633.
[35] C. M. Bates, A. B. Chang, N. Momčilović, S. C. Jones, R. H. Grubbs, *Macromolecules* **2015**, *48*, 4967–4973.
[36] T. Pakula, Y. Zhang, K. Matyjaszewski, H.-i. Lee, H. Boerner, S. Qin, G. C. Berry, *Polymer* **2006**, *47*, 7198–7206.
[37] Q. Pan, D. Barbash, D. M. Smith, H. Qi, S. E. Gleeson, C. Y. Li, *Adv. Energy Mater.* **2017**, *7*, 1701231.
[38] Z. Zhou, R. Zou, Z. Liu, P. Zhang, *Giant* **2021**, *6*, 100056.
[39] K. M. Diederichsen, H. G. Buss, B. D. McCloskey, *Macromolecules* **2017**, *50*, 3831–3840.
[40] O. Borodin, G. D. Smith, *Macromolecules* **2007**, *40*, 1252–1258.
[41] P. Bennington, C. Deng, D. Sharon, M. A. Webb, J. J. de Pablo, P. F. Nealey, S. N. Patel, *J. Mater. Chem. A* **2021**, *9*, 9937–9951.
[42] D. Diddens, A. Heuer, O. Borodin, *Macromolecules* **2010**, *43*, 2028–2036.
[43] M. A. Webb, Y. Jung, D. M. Pesko, B. M. Savoie, U. Yamamoto, G. W. Coates, N. P. Balsara, Z.-G. Wang, T. F. Miller, *ACS Cent. Sci.* **2015**, *1*, 198–205.
[44] O. Borodin, G. D. Smith, *Macromolecules* **1998**, *31*, 8396–8406.
[45] C. Deng, M. A. Webb, P. Bennington, D. Sharon, P. F. Nealey, S. N. Patel, J. J. de Pablo, *Macromolecules* **2021**, *54*, 2266–2276.
[46] L. Fetters, D. Lohse, R. Colby, in *Physical properties of polymers handbook*, (Ed: J. E. Mark), Springer, New York, NY, USA **2007**, 447–454.
[47] C. Zuo, B. Zhou, Y. H. Jo, S. Li, G. Chen, S. Li, W. Luo, D. He, X. Zhou, Z. Xue, *Polym. Chem.* **2020**, *11*, 2732–2739.
[48] W. Wei, Z. Xu, L. Xu, X. Zhang, H. Xiong, J. Yang, *ACS Appl. Energ. Mater.* **2018**, *1*, 6769–6773.
[49] Q. Lu, Y.-B. He, Q. Yu, B. Li, Y. V. Kaneti, Y. Yao, F. Kang, Q.-H. Yang, *Adv. Mater.* **2017**, *29*, 1604460.
[50] G. Pan, in *Physical properties of polymers handbook*, (Ed: J. E. Mark), Springer, New York, NY, USA **2007**, 577–584.
[51] R. A. Mantz, P. F. Jones, K. P. Chaffee, J. D. Lichtenhan, J. W. Gilman, I. M. K. Ismail, M. J. Burmeister, *Chem. Mater.* **1996**, *8*, 1250–1259.
[52] Y. Gao, Z. Yan, J. L. Gray, X. He, D. Wang, T. Chen, Q. Huang, Y. C. Li, H. Wang, S. H. Kim, T. E. Mallouk, D. Wang, *Nat. Mater.* **2019**, *18*, 384–389.

Manuscript received: October 29, 2021
Accepted manuscript online: November 9, 2021
Version of record online: November 17, 2021